

The Disk Substructures at High Angular Resolution Project (DSHARP) II: An overview of ringed substructures in protoplanetary disks

JANE HUANG¹ AND OTHERS

¹Harvard-Smithsonian Center for Astrophysics, 60 Garden Street, Cambridge, MA 02138, USA

ABSTRACT

Ring-like features are the most common type of substructure observed in DSHARP, the first high angular resolution ALMA survey of protoplanetary disks. We present an analysis of the eighteen protoplanetary disks around single stars. Ring-like substructures are observed in seventeen of these sources, and tentatively detected in the eighteenth.

-Remark on diversity of ring structures observed
 To be continued...

Keywords: protoplanetary disks—ISM: dust—techniques: high angular resolution

1. INTRODUCTION

In the past few years, moderate-to-high angular resolution ALMA observations have revealed concentric ring and gap structures in the millimeter continuum of a small but steadily growing number of protoplanetary disks (REFS).

small but steadily growing number of disks

Boilerplate

Ring-like substructures are the most common type of emission feature observed something something systematic study, something something trends.

2. SAMPLE OVERVIEW

We analyze high angular resolution 1.3 mm continuum observations of the eighteen disks around single stars from the DSHARP survey presented in Andrews et al. (in prep), hereafter DSHARP1. The stellar host properties and data calibration are described in DSHARP1.

All sources were imaged using the multi-scale multi-frequency synthesis algorithm (Cornwell 2008), as implemented in the `tclean` task in CASA v.5.1.1. The resulting images are shown in Figure ???. For each source, different Briggs weighting and gaussian *uv* taper parameters are tested with the aim of keeping sidelobe levels below ~ 15 percent and creating a relatively circular synthesized beam while maintaining sufficient angular resolution and sensitivity to recover the source substructure. In general, lower Briggs robust values were used for the very high signal-to-noise sources (e.g. AS 209, HD 163296) with bright, concentrated ring features, while higher values were favored for sources with low-level,

Table 1. Imaging parameters

Source	Briggs parameter	Taper	Synthesized beam
			mas × mas
AS 209	-0.5	37 × 10 (162°)	38 × 36 (68°0)
DoAr 25	0.5	-	48 × 27 (79°5)
DoAr 33	0	20 × 10 (-13°)	36 × 24 (75°1)
Elias 20	0	-	32 × 23 (76°3)
Elias 24	0	35 × 10 (166°)	36 × 34 (81°6)
Elias 27	0.5	40 × 20 (173°2)	49 × 47 (47°2)
GW Lup	0.5	35 × 15 (0°)	45 × 43 (0°5)
HD 142666	0.5	-	32 × 22 (61°6)
HD 143006	0	42 × 20 (172°1)	46 × 45 (51°3)
HD 163296	-0.5	-	48 × 38 (81°7)
IM Lup	0.5	33 × 26 (137°5)	44 × 43 (-64°9)
MY Lup	0	39 × 15 (162°7)	44 × 43 (-58°2)
RU Lup	-0.5	22 × 10 (6°)	25 × 24 (-51°0)
SR 4	-0.5	35 × 10 (0°)	34 × 34 (10°1)
Sz 114	0.5	-	67 × 28 (-88°0)
Sz 129	0	-	44 × 31 (-86°8)
WaOph 6	0	55 × 10 (9°8)	58 × 54 (84°3)
WSB 52	0	33 × 27 (74°1)	33 × 27 (74°1)

extended emission (e.g. IM Lup, GW Lup). The Briggs weighting parameters, Gaussian *uv* taper parameters (if applicable), and resulting synthesized beams for the images shown in Figure ?? are listed in Table 1.

(Author note: To what extent to include include MWC 758 (Dong), TW Hya (Andrews/Huang) and HL Tau in quantitative analysis?) (Author note: Where did we land on what name to use for Sz 114?)

3. DISK FEATURES

3.1. Radial locations of rings and gaps

Corresponding author: Jane Huang
 jane.huang@cfa.harvard.edu

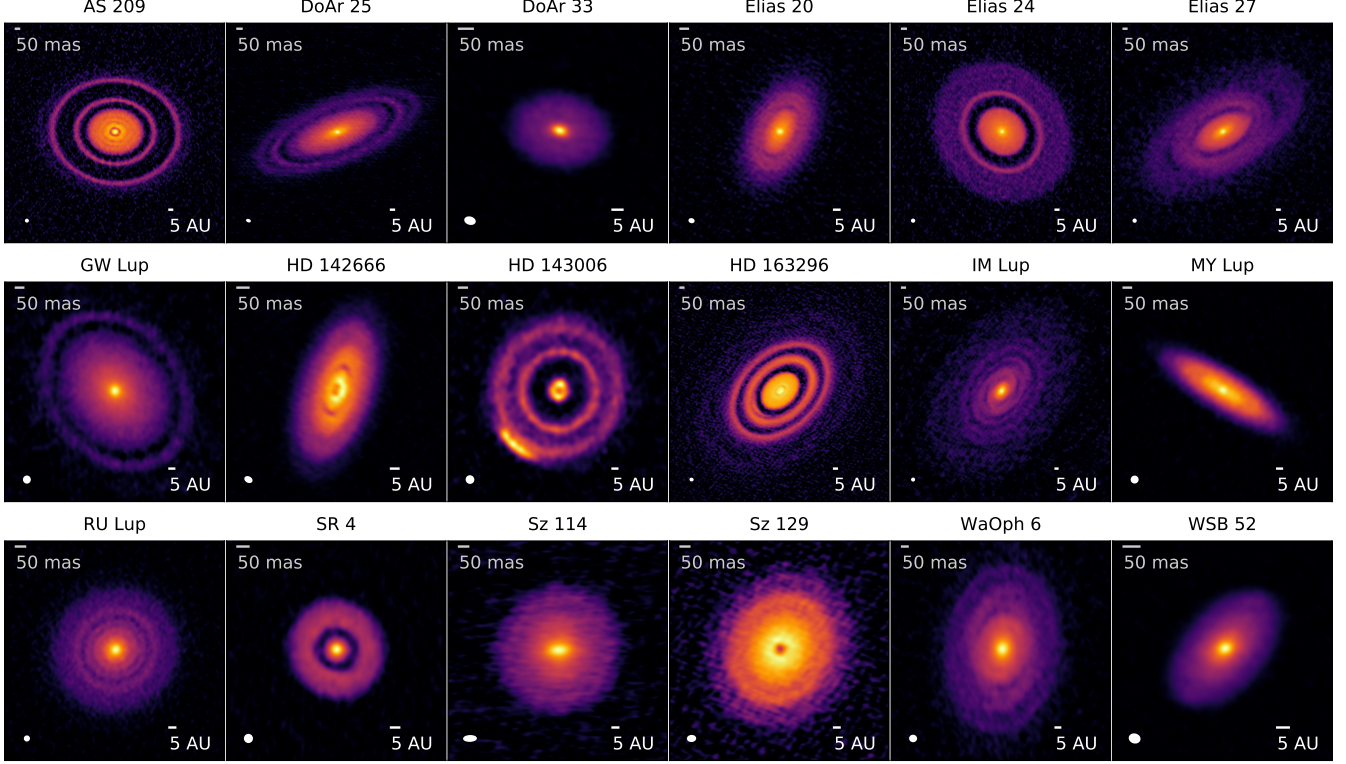


Figure 1. ALMA 1.3 mm continuum observations of the 18 protoplanetary disks around single stars from DSHARP. Synthesized beams are drawn in the lower left corner. An individualized arcsinh stretch is applied to each disk to increase the visibility of the substructures in the outer disk regions, with the minimum value set to zero and the maximum value set to the maximum pixel value. Bars are shown for the angular and linear scales, adopting the [Gaia Collaboration et al. \(2016\)](#) distances listed in Table 1 of DSHARP1.

Annular features are labeled with the prefix “DA” (for Dark Annulus) followed by the radial location of the ring rounded to the nearest whole number if the feature corresponds either to a local minimum in the radial profile or if the radial component of the gradient sharply transitions from steeply decreasing to nearly flat. Colloquially, such features are often referred to as “gaps” in the literature (e.g [ALMA Partnership et al. 2015](#); [Isella et al. 2016](#); [Fedele et al. 2017](#)), although use of this term should not be construed to imply that they necessarily formed via some kind of clearing mechanism. Similarly, annular features are labeled with the prefix “BR” (for Bright Ring) followed by their radial locations if the feature corresponds either to a local maximum in the radial profile or to locations where the radial component of the gradient transitions from being nearly flat to being steeply decreasing.

The positions of the most distinct annular features are measured in a manner similar to that employed for the HL Tau disk in ALMA Partnership ([ALMA Partnership et al. 2015](#)). A preliminary deprojection of each disk image is performed using estimates of the disk orientation from either a Gaussian fit to the image or from existing literature measurements (REF Fedele for AS 209, Dip-

ierro for Elias 24, Andrews et al. (submitted) for Sz 129, Sz 114, GW Lup). Radial cuts of the image are then taken along evenly spaced azimuthal angles, where the spacing for each feature is set to be on the order of the synthesized beam size to ensure that the different cuts are largely independent. For each radial cut, we search for a local extremum in the vicinity of the observed disk feature, generally using a search window of ~ 6 to 20 AU depending on the apparent width of the feature. If an extremum is not present in a given radial cut (either because of insufficient angular resolution arising from the disk projection or from low signal-to-noise), that azimuthal angle is excluded from measurement. For the Elias 27 disk, the azimuthal angles where the spiral arms cross the gap are excluded. When fitting ellipses to the features labeled BR65 in the HD 143006 disk, the azimuthal angles occupied by the asymmetry on the southeast side are excluded.

Ellipses are then fit to the pixel coordinates extracted for each ring. The likelihood takes the form

$$\log L = , \quad (1)$$

where d is the orthogonal distance of the measured coordinate from the model ellipse, and σ is the standard

deviation of the orthogonal distances. The formulae for calculating the orthogonal distances from an ellipse are provided in (Zhang 1997). Six parameters are fit for: the offset of the ellipse center from the phase center (Δx and Δy), the semimajor axis of the ellipse (r_0), the ratio of the lengths of the semiminor to semimajor axes ($\cos i$), the position angle, and the natural log of the variance in the orthogonal distance offsets of the measured ellipse points from the presumed true ellipse ($\log \sigma^2$). Flat priors are specified for Δx , Δy , r_0 , and $\log \sigma^2$. Gaussian priors for $\cos i$ and PA were specified for AS 209 based on measurements in REF, Elias 24 based on REF, and Sz 129, Sz 114, and GW Lup from (REF). For disks where previous measurements of PA and inclination were not available, conflicting, or visibly inaccurate, flat priors for $\cos i$ and PA are adopted. The posterior is sampled using emcee (REF, and list the chain length, number of walkers, burn-in, and convergence criteria). The posterior medians are listed in Table 2, with error bars calculated from the 16th and 84th percentiles. The position angles and inclinations of the disks, listed in Table 3 were computed by taking weighted averages of the measurements for the individual annular features.

For the disks where the annular substructure is not sufficiently high contrast to fit ellipses directly (WSB 52, MY Lup, DoAr 33, HD 142666), position angles and inclinations are computed by fitting elliptical gaussians to the images using the `imfit` task in CASA and listed in Table 3. Even if the intensity profile deviates from a gaussian, a gaussian fit should still match the position angle and inclination of the source provided that the source is axisymmetric and the overall extent of the disk is well-resolved (REF). To check that the gaussian fitting procedure yields reasonable results, position angles and inclinations were also calculated for the disks with well-defined rings and compared to the results from the ellipse-fitting method, which generally agreed within one degree.

Radial profiles were then calculated for each disk by deprojecting the disk, then binning the pixels in annuli one AU wide and averaging the intensities in each bin. For most disks, the average is taken through all azimuthal angles. For HD 143006 and HD 163296, angles where the emission asymmetry is visible are excluded from the calculation. For disks with very high inclination (Elias 20, DoAr 25, MY Lup, WSB 52, and HD 142666), only azimuthal angles that are within 20 degrees (as measured in deprojected coordinates) of the major axis of the projected disk image are included in the average, since the emission structures are not well-resolved along the minor axis.

The radial locations of additional ringlike substructures are identified by searching for local maxima and minima in the averaged radial profiles and cross-referenced with the original image to verify that they correspond to annular features, since non-axisymmetric features such as spiral arms can also create local extrema in the radial profile. The uncertainty on the radial location is estimated as the width of the radial bin. The radial locations of ring-like substructures that do not correspond to formal local maxima and minima are estimated through visual inspection of the radial profile and image. Because this is somewhat subjective, the locations are given as approximations without formal error estimates, but the accuracy of the estimate should be on the order of the scale of the synthesized beam. These locations are also listed in Table 2.

In addition, additional annular features of interest in the disk are identified with the label “CF” (for Circular Feature) followed by the estimated radial location. Most of these features correspond to breaks or shoulders in the intensity profile that may correspond to the inward edge of a gap or be associated with dust evolution (e.g. Hogerheijde ref). Other features of interest are possible gaps and rings in disks where the spiral arms create ambiguity in the classification. of the additional “features of interest,” their radial locations

Table 2. Positions and orientations of emission rings and gaps

Source	Feature	Δx	Δy	Semi-major axis	Semi-major axis	Inclination	Position Angle
(1)	(2)	(mas)	(mas)	(arcsec)	(AU)	(degrees)	(degrees)
AS 209	DA9	3 ± 1	-3.9 ± 0.9	0.0718 ± 0.0008	8.69 ± 0.11	$35.6_{-0.8}^{+0.7}$	85.7 ± 0.7
	BR14	1.9 ± 1.3	$-4.1_{-1.2}^{+1.1}$	$0.1186_{-0.0011}^{+0.0010}$	14.35 ± 0.14	35.1 ± 0.7	85.7 ± 0.7
	DA24	$2.5_{-1.5}^{+1.4}$	-4.2 ± 1.3	0.1964 ± 0.0013	$23.77_{-0.15}^{+0.16}$	35.4 ± 0.7	$85.9_{-0.6}^{+0.7}$
	BR28	5 ± 2	-5 ± 2	0.230 ± 0.002	$27.8_{-0.3}^{+0.2}$	35.0 ± 0.7	86.2 ± 0.7

Table 2 continued

Table 2 (*continued*)

Source	Feature	Δx	Δy	Semi-major axis	Semi-major axis	Inclination	Position Angle
		(mas)	(mas)	(arcsec)	(AU)	(degrees)	(degrees)
(1)	(2)	(3)	(4)	(5)	(6)	(7)	(8)
	DA35	5±1.5	-3±1.3	0.2888±0.0014	34.95±0.16	35.6±0.6	85.7 ^{+0.6} _{-0.7}
	BR38	2±2	-3±2	0.318±0.002	38.4±0.3	34.3±0.7	85.70.7
	DA61	-3±3	-4±2	0.505 ^{+0.2} _{-0.3}	61.0±0.3	36.0±0.6	86.0±0.6
	BR74	-0.7±1.1	-4.2±1	0.6112±0.0013	73.96 ^{+0.12} _{-0.13}	34.6±0.3	85.7 ^{+0.5} _{-0.4}
	DA90	2±3	-7±3	0.7453±0.003	90.0±0.3	34.4±0.5	86.2±0.6
	BR99	7±3	-3±3	0.8165 ^{+0.0035} _{-0.0033}	98.8±0.4	34.1±0.5	85.9 ±0.6
	DA105	-4±3	-2±3	0.870±0.003	105.2±0.4	34.3±0.5	86.0 ±0.6
	BR120	-0.1±0.12	1.7±1.1	0.9938 ^{+0.0014} _{-0.0015}	120.3±0.13	35.0±0.2	85.7±0.3
	DA137				137±1		
	BR141				141±1		
DoAr 25	DA76				~76		
	BR85				~85		
	DA97	40±3	-49±2	0.702±0.004	96.8±0.3	67.4±0.3	110.5±0.3
	BR111	35±3	-49±3	0.804±0.004	110.9±0.3	66.1±0.3	110.1±0.3
	DA125				125±1		
	BR137				137±1		
DoAr 33	DA8			~ 0.06	~ 8		
	BR16			~ 0.15	~ 16		
Elias 20	DA25	-54.4±1.5	-491 ^{+0.0012} _{-0.0013}	0.1816 ^{+0.0016} _{-0.0015}	25.1±0.2	49±1	153.2±1.3
	BR29				29±1		
	DA33				33±1		
	BR36				36±1		
	DA45				45±1		
Elias 24	DA57	110±2	-386±2	0.418±0.002	56.8±0.3	27.7±0.9	51±2
	BR77	111±1	-387±1	0.5641 ^{+0.0012} _{-0.0011}	76.71±0.13	29.2±0.4	45.2±0.8
	DA89			0.654±0.007	89±1		
	BR123			0.904±0.007	123±1		
Elias 27	DA69	-6±4	-7±3	0.594 ^{+0.7} _{-0.6}	68.9±0.4	55.9 ^{+0.7} _{-0.8}	118.7±0.7
	BR87				87±1		
GW Lup	DA74	-2.5 ^{+1.6} _{-1.4}	0.8±1.5	0.479±0.002	74.3±0.2	38.8 ^{+0.4} _{-0.5}	37.7 ^{+0.8} _{-0.7}
	BR85	-2.3±0.2	1±2	0.551±0.002	85.4±0.3	38.8 ^{+0.4} _{-0.5}	37.6±0.8
	DA102			0.658±0.006	102±1		
	BR108			0.697±0.006	108±1		
HD 142666	DA2			0.014	2 ± 1		
	BR6			0.04	6±1		
	DA16			0.11	16±1		
	BR20			0.14	20±1		

Table 2 continued

Table 2 (*continued*)

Source	Feature	Δx (mas)	Δy (mas)	Semi-major axis (arcsec)	Semi-major axis (AU)	Inclination (degrees)	Position Angle (degrees)		
		(1)	(2)	(3)	(4)	(5)	(6)	(7)	(8)
	DA35					~ 35			
	BR41					~ 41			
	DA54					~ 54			
	BR58					~ 58			
HD 143006	BR6					6 ± 1			
	DA24					24 ± 1			
	BR41	-6.3 ± 0.6	21.5 ± 0.6	0.2472 ± 0.0008	40.8 ± 0.1	18.9 ± 0.9	169 ± 3		
	DA52					52 ± 1			
	BR65	-1 ± 2	24 ± 2	0.393 ± 0.3	64.9 ± 0.4	17 ± 2	164^{+7}_{-6}		
HD 163296	DA10					10 ± 1			
	BR14					14 ± 1			
	DA48					48 ± 1			
	BR67	-4.3 ± 1.3	6.7 ± 1.2	$0.6638^{+0.0015}_{-0.0016}$	67.04 ± 0.12	46.9 ± 0.2	133.4 ± 0.3		
	DA86	1 ± 3	2 ± 3	0.855 ± 0.004	86.4 ± 0.3	46.9 ± 0.4	132.6 ± 0.5		
	BR100	-2.3 ± 0.9	9.0 ± 0.9	0.9870 ± 0.0011	99.69 ± 0.09	46.63 ± 0.12	133.36 ± 0.17		
	DA142					142 ± 3			
	BR155					155 ± 1			
IM Lup	DA118	-1 ± 3	-3 ± 3	0.744 ± 0.004	117.6 ± 0.5	47.3 ± 0.6	145.2 ± 0.8		
	BR133	0 ± 3	0 ± 3	0.844 ± 0.004	133.4 ± 0.5	47.5 ± 0.5	144.2 ± 0.6		
MY Lup	DA30			~ 0.19		~ 30			
	BR40			~ 0.26		~ 40			
RU Lup	DA14			~ 0.088		~ 14			
	BR17			~ 0.107		~ 17			
	DA22			0.138 ± 0.006		22 ± 1			
	BR24			0.159 ± 0.006		24 ± 1			
	DA29	-17 ± 1	88 ± 1	$0.1829^{+0.0014}_{-0.0015}$	29.1 ± 0.2	20 ± 2	118 ± 6		
	BR34	-17 ± 1	87 ± 1	0.214 ± 0.002	34.0 ± 0.2	16^{+2}_{-3}	123 ± 9		
	DA42			~ 0.264		~ 42			
	BR50			~ 0.314		~ 50			
SR 4	DA11					11 ± 1			
	BR19	-64 ± 3	-509 ± 3	0.140 ± 0.003	$18.9 \pm$	25^{+5}_{-6}	44^{+13}_{-12}		
Sz 114	DA39	0 ± 5	3 ± 4	0.238 ± 0.003	38.6 ± 0.6	21 ± 2	165 ± 7		
	BR45	-2 ± 3	4 ± 3	0.280 ± 0.003	45.4 ± 0.5	$21.7^{+1.4}_{-1.7}$	166 ± 5		
Sz 129	BR10			0.062 ± 0.006	10 ± 1				
	DA41	7 ± 3	4 ± 3	0.254 ± 0.003	40.9 ± 0.5	31.6 ± 0.9	154 ± 2		
	BR46	7 ± 3	4^{+2}_{-3}	0.285 ± 0.002	45.9 ± 0.4	32.0 ± 0.9	155 ± 2		
	DA63			0.391 ± 0.006	64 ± 1				

Table 2 continued

Table 2 (*continued*)

Source	Feature	Δx	Δy	Semi-major axis	Semi-major axis	Inclination	Position Angle
		(mas)	(mas)	(arcsec)	(AU)	(degrees)	(degrees)
(1)	(2)	(3)	(4)	(5)	(6)	(7)	(8)
	BR66				0.410±0.006	66±1	
WaOph 6	DA80					80±1	
	BR88	-244±3	-361±3	0.712±0.004	87.5±4	47.2±0.7	174.2±0.8
WSB 52	DA22				~ 0.16	~ 22	
	BR25				~ 0.18	~ 25	

Table 3. Position angles and inclinations of disks

Source	P.A.	Incl.	method
	deg	deg	
AS 209	85.82±0.15	34.85±0.13	E
DoAr 25	110.3±0.2	66.8±0.2	E
DoAr 33	81.1±1.2	41.8±0.8	G
Elias 20	153.2±1.3	49±1	E
Elias 24	45.9±0.8	28.9±0.4	E
Elias 27	118.7±0.7	55.9 ^{+0.7} _{-0.8}	E
GW Lup	37.7±0.6	38.8±0.4	E
HD 142666	162.16±0.14	61.66±0.13	G
HD 143006	168.6±2	18.6±0.8	E
HD 163296	133.31±0.14	46.7±0.1	E
IM Lup	144.6±0.5	47.4±0.4	E
MY Lup	58.8±0.1	73.2±0.1	G
RU Lup	119±5	18.6±1.6	E
SR 4	44±13	24 ⁺⁴ ₋₆	E
Sz 114	165±4	21.4±1.3	E
Sz 129	154.5±1.2	31.8±0.6	E
WaOph 6	174.2±0.8	47.2±0.7	E
WSB 52	138.4±0.3	54.4±0.2	G

3.2. Non-axisymmetric structures

3.2.1. Azimuthal asymmetries

Within the uncertainties, the ringed substructures in the disks generally appear to be axisymmetric. There do not appear to be significant offsets measured between the centers of the ringed substructures in the disks.

- Comment on limits on asymmetry for other rings based on amount of scatter in radial bins

- Rings and gaps generally seem concentric but more reliable results would probably have to be derived by forward modeling

Table 4. Radial locations of circular features of interest

Source	Feature	Radius	Notes
		arcsec	
DoAr 25	CF63	~ 0.46	Shoulder in intensity profile leading into gap
Elias 20	CF20	~ 0.14	Shoulder in intensity profile leading into gap
Elias 24	CF14	~ 0.10	Slope decrease in intensity profile
	CF42	~ 0.31	Shoulder in intensity profile leading into gap
Elias 27	CF125	~ 1.08	Possible gap intersected by spiral arms
GW Lup	CF10	~ 0.07	Slope decrease in intensity profile
	CF65	~ 0.42	Shoulder in intensity profile leading into gap
IM Lup	CF98	Either a ring or tightly-wrapped spiral	
MY Lup	CF8	~ 0.05	Divot in intensity profile
HD 163296	CF20	Divot in intensity profile	
	CF33	Shoulder in intensity profile leading into gap	

Note that the DA9 feature in AS 209 and DA11 feature in SR4 appear to have “gap-crossing” emission that arises as a consequence of the PSF sidelobes.

Two sources, HD 143006 and HD 163296, have crescent-shaped azimuthal asymmetries near well-defined rings. HD 143006 exhibits a bright feature These sources are G and A stars, respectively, which fits in with the trend of asymmetric disks being observed predominantly around stars with earlier spectral types (REF). The nature of these asymmetries is explored in further detail in Isella et al. (in prep) for HD 163296 and Pérez et al. (in prep) for HD 143006. -briefly comment on contrast level of asymmetry

The peak of the continuum emission of HD 163296 is also offset from the measured centers of the BR67 and BR100 rings by ~XX arcseconds (YY AU). -HD 142666 and HD 163296 have asymmetries in the inner disk that are most likely due to vertical structure (slash shadowing?)

Spiral arms are another notable type of non-axisymmetric structure, seen in three of the disks that have ringed substructures (WaOph 6, IM Lup, and Elias 27). See Huang et al. (in prep) for further analysis of the spiral structures.

3.3. Trends in the morphology of ringlike substructures

Figure 2. Deprojected and azimuthally averaged radial profiles on a linear scale. The light blue ribbon shows the 1σ scatter of each radial bin. Vertical lines mark the features described in Table 2. The Gaussian profile shows the FWHM of the minor axis of the synthesized beam.

Figure 3. Same as Figure 2, but with the intensities on a log scale.

Figure 4. Deprojected disk images with features labeled.

Figure 5. Brightness temperature profiles (maybe additional annotations for snowline discussion?)

Figure 6. Some kind of histogram of the distribution of rings and gaps?

-rings and gaps occur as far in as x and as far out as y
y -spacings occur as small as x and as large as y
Zhang commonality paper

3.3.1. Possible resonances

The relative positions of certain pairs of gaps and rings appear to be consistent with mean-motion resonances.
BR65:BR41 in HD 143006 pretty much exactly 2:1 period ratio

DA29:DA22:DA14 in RU Lup could be 3:2:1
BR155:BR100 in HD 163296 could be 2:1
DA89:DA57 in Elias 24 could be 2:1
BR187:BR85 in DoAr 25 could be 2:1
DA63:DA41 in Sz 129 could be 2:1
BR120:BR74 in AS 209 could be 2:1 -also period ratio histogram

3.3.2. Gap contrast levels

Six disks exhibit well-resolved gap-like features that appear to be essentially devoid of millimeter continuum emission: GW Lup, AS 209, HD 143006, HD 163296, Elias 24, and DoAr 25. Their host stars are diverse, ranging from spectral types M through A, and spanning an order of magnitude in luminosity and several orders of magnitude in accretion rates. These “deep gaps” occur across a range of radii, from 24 AU in HD 143006 to 105 AU in AS 209, and their positions do not exhibit an obvious trend with stellar parameters. One possible pattern is that these disks are among the largest in the sample, with all except HD 143006 exhibiting continuum emission beyond a radius of 100 AU. However, while DA11 is not completely devoid of emission in SR 4, one of the smallest disks observed, it is one of the highest contrast gaps observed in the survey. In addition, two of the largest disks, Elias 27 and IM Lup, appear to have relatively low contrast annular features, although they also have spiral arms and may therefore Further observations of disks across a range of sizes will be necessary to investigate trends with gap depths.

-comment on gaps wider than rings vs rings wider than gaps -But a lot of gaps seem pretty shallow. Emphasize need for high sensitivity?

3.4. Remarks on individual sources

We comment on the results for individual sources and draw comparisons with other millimeter continuum, scattered light, and molecular line observations from the literature. Unless otherwise noted, the features remarked upon are resolved for the first time in this survey.

3.4.1. AS 209

3.4.2. DoAr 25

DoAr 25 hosts an extended, high inclination disk with three pairs of annular gaps and rings. Integration time shorter for this disk. Tentative additional rings in inner disk. Need higher res to confirm. Reference Cox paper, Weaver et al. in prep.

3.4.3. Elias 20

Maybe one of the gaps should be called a tentative gap instead?

3.4.4. Elias 24

Tentative additional rings Cox, Dipierro, Cieza papers

3.4.5. Elias 27

Prominent gap at See Huang et al. (in prep) for analysis of the spiral geometry. Comment on extinction?

3.4.6. HD 142666

At first I thought there was a central cavity, but now I think there must be a smaller inner disk

Recent paper inferring gap REF

3.4.7. HD 143006

HD 143006 hosts a nearly face-on disk consisting of three narrow rings separated by wide gaps. A central cavity/clearing is visible but not well-resolved. The most striking feature is the asymmetry on the southeast side of the outermost ring, noted previously in Barenfeld et al. (REF). See Pérez et al. (in prep.) for further analysis of HD 143006. Discuss Myriam’s paper.

3.4.8. HD 163296

Image peak is off center Almost looks like an unresolved version of HD 142666, which has a gap Unclear if there are multiple gaps and rings at 140 AU

3.4.9. MY Lup

MY Lup hosts the most highly inclined disk in the survey. Although some studies have classified MY Lup as a transition disk (REFS), our ALMA image does not display a central cavity. However, there is radial substructure in the vicinity of where the cavity was previously inferred. Ref. Weaver et al. in prep

3.4.10. RU Lup

mention high activity of RU Lup

3.4.11. SR 4

PSF effects can be observed in the gap SR4 hosts one of the smallest disks in the sample. Because of the small size of the disk, the uncertainties on the disk viewing geometry are large.

3.4.12. Sz 114 (V908 Sco)

The disk around this T Tauri star features a marginally resolved gap at 38.6 AU, surrounded by an emission ring at 45.3 AU. Due to poor weather, the on-source integration time for this source was only about half as long as that for most of the sample. The comparatively low signal-to-noise, small radial extent of the disk, and low disk inclination lead to large uncertainties for the viewing geometry. However, because the disk is nearly face-on ($\cos i = 0.93$), the derived radial profile does not depend strongly on the inferred viewing geometry.

3.4.13. Sz 129

The direct imaging of a small central cavity in the Sz 129 disk confirms the tentative identification in Tazzari et al (REF) via visibility modeling of lower-resolution data.

3.4.14. WSB 52

There seems to be some kind of substructure but not clear whether it's a gap (high inclination and small size makes this difficult)

4. DISCUSSION

4.1. Comparison to other millimeter detections of protoplanetary disks

-Make the point that other observations by necessity were biased toward larger-scale structures

4.2. Prevalence of millimeter continuum substructures

Since DSHARP selected preferentially for bright protoplanetary disks, it is not straightforward to derive an occurrence rate for millimeter continuum substructures. Nevertheless, interesting lower bounds can still be set.

4.2.1. Disks in Lupus

4.2.2. Disks in Ophiuchus

4.2.3. Relation with stellar parameters

-Seen in a range of spectral types, but most of the disks observed so far are pretty bright, so the occurrence could be different if stellar mass/disk mass relationship is taken into account?

-No obvious trend seen so far with accretion rate, host star luminosity, host star age

-How early do these structures form? Comment on Class I disks

-Comment on Group I/Group II Herbig stars (Garufi 2017, Maaskant 2013)

4.2.4. Small versus large disks

make a point about the marginally resolved gaps

4.3. Possible origins of ringlike substructures

4.3.1. Planets

-Discuss the various hydro papers (start with Lin and Papaloizou and keep going)

-Discuss previously proposed protoplanets for AS 209, HD 163296, Elias 24 (Isella, Teague, Pinte, Fedele, Dipierro)

Of the DSHARP targets, the companion hypothesis has been investigated most extensively for the HD 163296 disk. Guidi et al. (2018) reported the detection of a point source in L' band within the DA48 feature, although further observations will be necessary to establish whether the source is a protoplanet. Pinte et al. (2018) also present kinematic evidence for a $\sim 2 M_J$ protoplanet at a radius of ~ 260 AU, which lies outside the detected continuum emission

-Discuss previous companion searches and limits

Exoplanetary system architectures have been observed to be diverse (e.g. Winn & Fabrycky 2015), which would perhaps

While direct imaging will be useful for detecting the high-mass sources

Comment on GAS Elias 24 and Elias 27 - cloud contamination. Deep gaps are the best candidates to search because of the contrast issues. AS 209, HD 163296, HD 143006

Mention Teague's CS paper to comment on alternative tracers for Elias 24 and Elias 27 REF to Shangjia's and Kees's papers.

4.3.2. Snowlines

-Discuss Zhang, Okuzumi, Pinilla -Comment on brightness temperatures and optical depth? -point out that GW Lup gap seems way too far out to be snowline related -caveat: thermal evolution of disk?

(Author note: Get Karin's input on this part)

4.4. Photoevaporation

Three of the disks in the sample (HD 143006, HD 142666, and Sz 129) exhibit small central cavities, although the angular resolution is not sufficient to determine whether they are cleared of material. X-ray photoevaporation has been proposed as a mechanism for dispersing disks from the inside-out (e.g.).

4.5. Dead zones

Discuss Flock, Ruge, Pinilla papers (**Author note: Get Xuening's input on this part**)

4.5.1. Other hypotheses

- Secular gravitational instability
- Dipierro back reaction
- Streaming instability
- photoevaporation for small cavities (Owen and Clarke)
- etc
- Some sort of plot related to cumulative flux distributions
- Histograms as functions of stellar properties

5. SUMMARY

REFERENCES

- ALMA Partnership, Brogan, C. L., Pérez, L. M., et al. 2015, ApJL, 808, L3
- Astropy Collaboration, Robitaille, T. P., Tollerud, E. J., et al. 2013, A&A, 558, A33
- Cornwell, T. J. 2008, IEEE Journal of Selected Topics in Signal Processing, 2, 793
- Fedele, D., Carney, M., Hogerheijde, M. R., et al. 2017, A&A, 600, A72
- Gaia Collaboration, Brown, A. G. A., Vallenari, A., et al. 2016, A&A, 595, A2
- Guidi, G., Ruane, G., Williams, J. P., et al. 2018, MNRAS, 1570
- Isella, A., Guidi, G., Testi, L., et al. 2016, Physical Review Letters, 117, 251101

This paper makes use of ALMA data [ADS/JAO.ALMA#2016.1.0](#). We thank the NAASC and JAO staff for their advice on data calibration and reduction. ALMA is a partnership of ESO (representing its member states), NSF (USA) and NINS (Japan), together with NRC (Canada) and NSC and ASIAA (Taiwan), in cooperation with the Republic of Chile. The Joint ALMA Observatory is operated by ESO, AUI/NRAO and NAOJ. The National Radio Astronomy Observatory is a facility of the National Science Foundation operated under cooperative agreement by Associated Universities, Inc. J.H. acknowledges support from the National Science Foundation Graduate Research Fellowship under Grant No. DGE-1144152 and from NRAO Student Observing Support.

Software: CASA ([McMullin et al. 2007](#)), SciPy, NumPy, Matplotlib, AstroPy ([Astropy Collaboration et al. 2013](#)), analysisUtils (https://casaguides.nrao.edu/index.php/Analysis_Utils), emcee, scikit-image

Facilities: ALMA